PROCEEDINGS OF SPIE

SPIEDigitalLibrary.org/conference-proceedings-of-spie

Optical properties of nematic microlenses doped with chiral nanoparticles

Perera, K., Nemati, A., Mann, E., Hegmann, T., Jákli, A.

K. Perera, A. Nemati, E. Mann, T. Hegmann, A. Jákli, "Optical properties of nematic microlenses doped with chiral nanoparticles," Proc. SPIE 11472, Liquid Crystals XXIV, 1147200 (20 August 2020); doi: 10.1117/12.2568570



Event: SPIE Organic Photonics + Electronics, 2020, Online Only

Optical properties of nematic microlenses doped with chiral nanoparticles

K. Perera¹, A. Nemati^{2,3}, E. Mann^{1,3}, T. Hegmann^{2,3,4,5} and A. Jákli^{1,2,3}

¹Physics Department, Kent State University, Kent OH, 44242, USA

² Advanced Materials and Liquid Crystal Institute Kent State University, Kent OH, 44242, USA

³ Materials Science Graduate Program, Kent State University, Kent OH, 44242, USA

⁴ Department of Chemistry and Biochemistry, Kent State University, Kent OH, 44242, USA

⁵ Brain Health Research Institute, Kent State University, Kent OH, 44242, USA

ABSTRACT

Nematic liquid crystals of achiral molecules or racemic mixtures of chiral ones form flat films and show uniform textures between circular polarizers when suspended in sub-millimeter size grids and submersed under water. Recently it was shown that on addition of chiral dopants to the liquid crystal, the films exhibit optical textures with concentric ring patterns with radial variation of the birefringence color, while the films become biconvex. The curved shape together with degenerate planar anchoring leads to a radial variation of the optical axis along the plane of the film, providing a Pancharatnam-Berry type phase lens that dominates the imaging.

Here we describe preliminary results of nematic liquid crystal microlenses formed by the addition of chiral nanoparticles. It is found that the helical twisting power of the nanoparticles, the key factor to form the lens, is an order of magnitude greater than that of the strongest molecular chiral dopants. From the observations we present here, we were able to estimate the shape and the geometric focal length of the lens and demonstrated its performance as an optical device. The use of chiral nanoparticles to make microlenses may allow tuning by light that the nanoparticles absorb or, for magnetic NPs, by magnetic fields. Further, the measurement of focal length at known NP concentration offers a new method to measure the helical twisting power of chiral nanoparticles.

Keywords: Liquid Crystals, Microlenses, Chirality, Nanoparticles

1. INTRODUCTION

Microlenses have applications ranging from biomimetic optical systems¹ to security printing ² and solar concentrators³. The most commonly-used solid microlenses are made through delicate fabrication processes^{4,5} and require mechanical adjustments to focus the image. In liquid lenses, the focal length is varied by electrowetting ^{6–10}. Liquid crystals (LC) can also be used to make lenses either by filling¹¹ or imprinting LCs in curved substrates^{12,13}, by using a LC film with constant thickness but spatially-varying refractive indices^{14–16}, or by creating regular defects by photolithography¹⁷. The common feature of all these microlenses is the requirement for delicate fabrication processes.

Recently Popov et al studied chiral nematic (N*) liquid crystals suspended in TEM grids when they were fully immersed in water. The observed polarized optical images (POM) between left and right circular polarizers revealed that the suspended chiral nematic liquid crystal films spontaneously form converging spherical microlenses. ¹⁸ Their results are summarized in Figure 1. Figure 1(a) shows the molecular structures of the studied liquid crystal pentyl cyano biphenyl (5CB) and the chiral dopant (CD) with helical twisting power (H.T.P.~8µm⁻¹ (top), the POM image of the LC with 3wt% CD (middle) and the sketch of the side view of the corresponding director structure (bottom). The experimental setup using an inverted Polarizing microscope is illustrated in Figure 1(b). The LC sample suspended in TEM grids immersed fully in water is placed between either left-, and right-handed circular polarizers, or crossed linear polarizers is viewed by the objective of the microscope that was equipped with a CCD camera. The geometric optic ray tracing of the convex LC lens (top) and the top view of the LC director arrangement determined by the optical measurement (bottom) are shown in Figure 1(c).

Liquid Crystals XXIV, edited by Iam Choon Khoo, Proceedings of SPIE Vol. 11472, 1147200 · © 2020 SPIE · CCC code: 0277-786X/20/\$21 doi: 10.1117/12.2568570

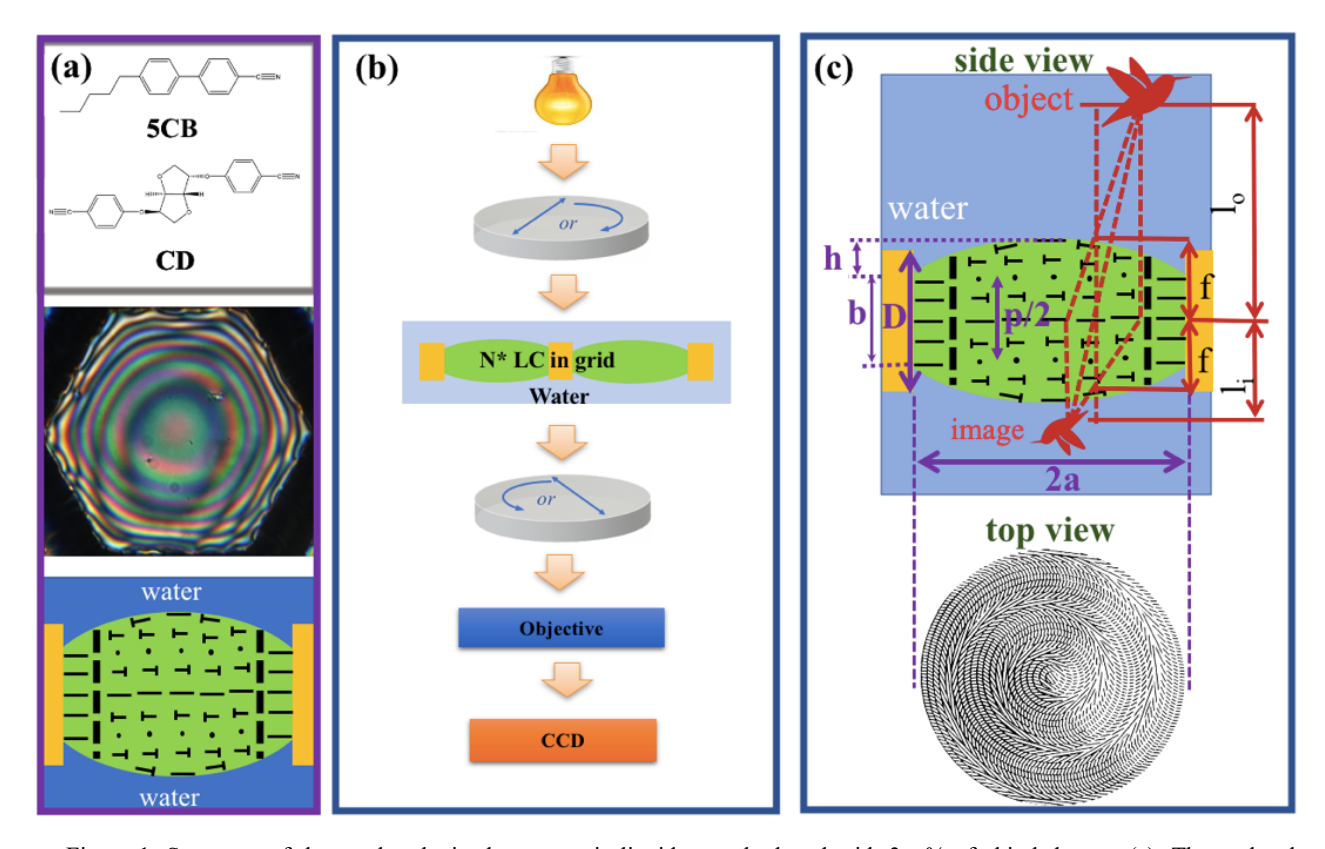


Figure 1: Summary of the results obtained on nematic liquid crystals doped with 3wt% of chiral dopant. (a): The molecular structures of the studied liquid crystal pentyl cyano biphenyl (5CB) and the chiral dopant (CD) with helical twisting power (H.T.P.~10µm⁻¹ (top), POM image of the LC with 3wt% CD (middle) and the sketch of the side view of the corresponding director structure (bottom). (b): Sketch of the experimental setup using inverted Polarizing microscope. The LC sample suspended in TEM grids immersed fully in water is placed between left-, and right-handed circular polarizers, or crossed linear polarizers is viewed by the objective of the microscope that was equipped by a CCD camera. (c): Schematics of the ray tracing of the convex LC lens (top) and the top view of the LC director arrangement.

The curvature radius R of the spherical cap LC lens was determined with good agreement both by comparing the birefringence color variation of the set of concentric colored rings (see the POM image in Figure 1(a)) and from the position of the consecutive interference fringes that appear even without polarizers. The Lensmaker's equation $(\frac{1}{f} \approx \frac{n_{lc} - n_w}{n_w} \frac{2}{R})$,

where f is the focal length, $n_{lc} \approx 1.7$ and $n_{w} \approx 1.33$ are the refractive indices of the liquid crystal and water, respectively) gave the focal lengths about 5-times larger than was obtained using the measured l_o and l_i object and image distances and geometric optic $(1/f_G = 1/l_o + 1/l_i)$. The contradiction was resolved by realizing that due to the degenerate planar anchoring at the water, the director rotates radially as the thickness changes (see top view of the director distribution sketched in the lower part of Figure 1(c). This variation results in a Pancharathnam-Berry (PB) phase lens and the actual focal length is due to the combination of closely-spaced geometric and PB lenses with $f = f_G \cdot f_{PB}/(f_G + f_{PB})$, where $f_p \approx \frac{p \cdot R}{8\lambda}$ is the focal length of the PB lens for a light with wavelength λ . Interestingly, such a spontaneously formed lens strongly resembles the radially varying optical axis of the compound eye of insects, such as the corneal lens structure of firefly compound eye²⁰⁻²². This may suggest that the chirality of the chitin and the aqueous environment are also important in the formation of the compound eyes.

The pressure difference needed for lens formation is due to the pseudo-layered structure of the chiral nematic material and the lensing is driven by the unwinding elastic energy near the TEM grid, which promotes uniform alignment perpendicular to the wall. The positive energy related to the unwinding of the helix near the wall is decreased by reducing the thickness of the LC-wall D by ΔD . The height of the spherical caps h is determined by the minimization of the

interfacial and wall energy with respect to h as $\frac{\partial (W_w + W_i)}{\partial h} = 0$. This yields $h \approx \frac{3\pi^2 K_{22} aD}{\gamma p^2 (\pi + 6)}$, where K_{22} is the twist elastic constant, p is the pitch of the helix and γ is the water-LC interfacial tension. The height of the spherical cap determines the curvature radius of the lens R as $R = a^2/(2h)$ and thus the focal length of the lens, as both f_G and f_{PB} are proportional to R. Remarkably R is proportional to the square of the helical pitch, which can be tuned by the chiral dopant, temperature and even with UV light, as shown recently by Y. Li et al.²³

Experiments on the chirality transfer from chiral nanostructures as chiral dopants to nematic LCs indicated that chiral ligand-capped gold nanoparticles (Au NPs) outperform their organic molecular counterparts, inducing tighter p values at lower overall concentrations of the chiral molecules. In addition, such Au NPs perform this amazing feat consistently over larger distances, translating into larger chiral correlation lengths. Such enhancement of through-space chirality found support from recent examples of demonstrated long-range interactions between chiral molecules and plasmonic nanostructures as well as enhanced anisotropy (or Kuhn's dissymmetry) factors, g ($g = \Delta \varepsilon / \varepsilon$, where $\Delta \varepsilon$ and ε are the molar circular dichroism and molar extinction coefficient) for chiral molecules in the vicinity of plasmonic nanostructures. Recent experimental data provided additional evidence for the hypothesis that desymmetrization of a plasmonic nanostructure (substituting Au NPs for gold nanorods, GNRs) results in further through-space chirality enhancement. Here, chiral cholesterol-capped GNRs showed an aspect ratio-dependent chirality amplification, prompting their own helical assembly in the induced N*-LC host that was explained by a chiral feedback loop.

In this paper we will describe preliminary results about the optical properties of microlens arrays that form when nematic liquid crystals doped with chiral nanoparticles instead of molecular chiral dopants. We find that as low as 0.1wt% gold nanoparticles with chiral ligands can provide curvature comparable to 5wt% chiral dopant.

2. MATERIALS AND METHODS

The liquid crystal 5CB (see molecular structure in Figure 1(a) and 2(a)) was purchased from Merck and used without further purification.

For the preparation of the chiral nanoparticles (see Figure 2(a)) ligand *Chole-thiol* (0.13 mol) was added to HAuCl4.3H2O (0.15 mmol) dissolved in 5 mL freshly distilled Tetrahydrofuran (THF) under flowing N₂. The mixture was stirred for 30 min (700 r.p.m). Then, NaBH4 (0.76 mmol) dissolved in 5 mL DI water was added and the color rapidly changed to brown. The reaction mixture stirred overnight. Solvent was removed under reduced pressure then brown precipitate was dissolved in *iso*-propanol/chloroform = 19:1 and centrifuged (12,000 rpm, 15 min) twice. The solvents were removed under reduced pressure and the particles were dried under N2. The NPs, redispersed in DCM, were mixed with different concentration of 5CB under N2 at room temperature for 48 h. The synthesis of the chiral ligand was accomplished according to previously reported methods.²⁵

For TEM grids we used nickel hexagonal 50/100 mesh Veco folding TEM grids purchased from Ted Pella, Inc. Before each experiment, the TEM grid and microscope dish were cleaned in methanol with an ultrasonic cleaner (Branson B200). For all measurements, the TEM folding grid containing two halves was held by its empty part. One of the halves ("sample part") is required to suspend the LC films while the other one ("holding part") is simply used for manipulating the grid.

The water was purified by a PureLab Plus system (18.2 M Ω ·cm). An Olympus CK40 inverted polarizing optical microscope (POM) was used to observe the N* films. A QICAM Fast1394 CCD camera was mounted on the microscope to capture images and videos. The sample was held between circular polarizers with opposite handedness.

3. RESULTS

The lensing caused by 0.1 wt% chiral nanoparticles added to the nematic liquid crystal, 5CB is summarized in Figure 2 and Figure 3. Figure 2(a) shows the molecular structure of 5CB, the schematic illustration of the gold nanoparticles caped with chiral molecules and the molecular structure of the chiral ligand. Figure 2(b) presents the Transmission Electron Microscopy (TEM) image of the chiral NPs showing that their size is about 3 nm.

Figure 2(c) shows the POM image of the microlens array of 5CB with 0.3 wt% NP immersed in water and placed between right and left circular polarizers. The distance between two parallel edges of the hexagonal grids is $2a = 200 \mu m$.

One can see 13 more-or-less concentric rings similar to the image of 5CB with 5 wt% chiral dopant. Additionally, there is bands of various birefringence colors varying between the first order grey to second order purple (or even to second order green in the bottom left lens) clearly demonstrated increasing optical path difference. Due to planar anchoring at the water-LC interface, this corresponds to an increasing film thickness. Figure 2(d) shows the images of an inverted "OK" created by the lens array of LC+0.3wt% NP mixtures. We note that we were unable to take a picture of the object through the lens array, which blurred the picture of the object.

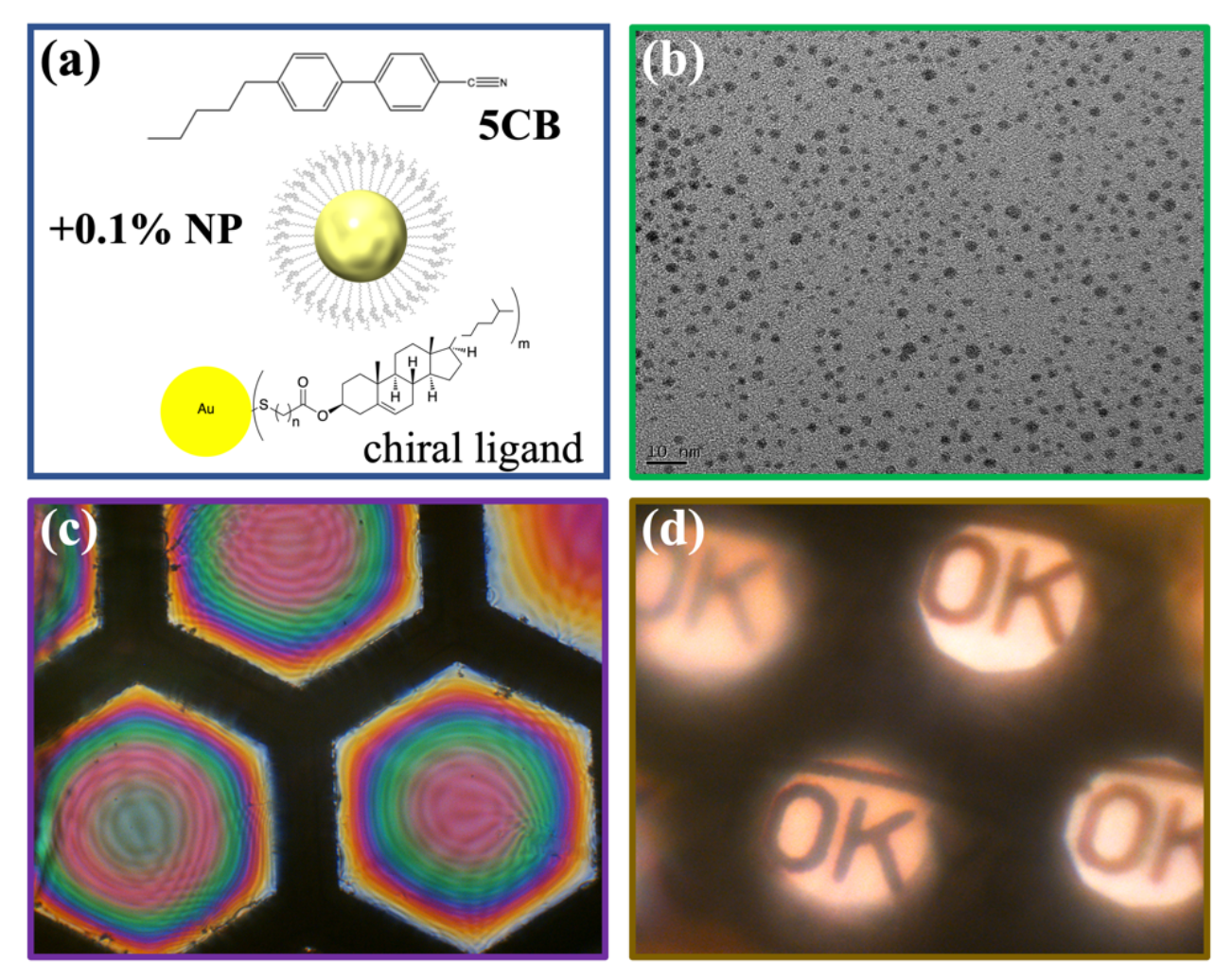


Figure 2: Summary of the lensing caused by chiral nanoparticles added to the nematic liquid crystal, 5CB. (a) The molecular structure of 5CB, schematic illustration of the gold nanoparticles caped with chiral molecules and the molecular structure of the chiral ligand. (b) Transmission Electron Microscopy image of the chiral NPs showing their size is about 3 nm. (c) POM image of the microlens array of 5CB with 0.3wt% NP immersed in water and placed between right and left circular polarizers. The distance between two parallel edges of the hexagonal grids is 2a=200μm. (d) Image of an inverted "OK" created by the LC+0.1wt% NP lenses shown in (c).

In order to be able to take a picture of the object as well as the image, we punctured every grid except one to leave only a single grid filled with the LC doped with the chiral NP. The result is shown in Figure 3(b), where both the object "40" and its image of the smaller inverted "40" can be seen for a 5CB+0.1wt% NP mixture. The relative sizes implies a magnification $M\sim1/4$. Figure 3(a) shows the POM image of the lens with 8 fringes; the same number as for 5CB 5wt% CD of $8\mu m^{-1}$ helical twisting power. This enables us to estimate the H.T.P. of the chiral nanoparticle to be about 400 μm^{-1} , which is much higher than the highest H.T.P. of molecular chiral dopants. Comparing the birefringence colors of the lens with the Michel-Levi chart shown below the POM image. The color varies between first order blue of $\Delta n \Delta D \sim 680$ nm at the edge up to second order purple of $\Delta n \Delta D \sim 1080$ nm. Assuming uniform birefringence $\Delta n \sim 0.15$, we estimate the

variation of the lens thickness of $\Delta D \sim 2.7 \, \mu m$. This enables us to estimate the curvature radius $R = a^2 / \Delta D \sim 3.7 \, mm$ and the focal length $f = \frac{R n_w}{2(n_{LC} - n_w)} \approx \frac{3.7 \cdot 1.33}{2(1.7 - 1.33)} \approx 6.7 \, mm$.

Detailed measurement results with various NP concentrations, measurements of the curvature radius from the distance of the interference fringes from the center of the lens, the image and object distances and discussion of the PB properties of the lenses will be subject of future publication.

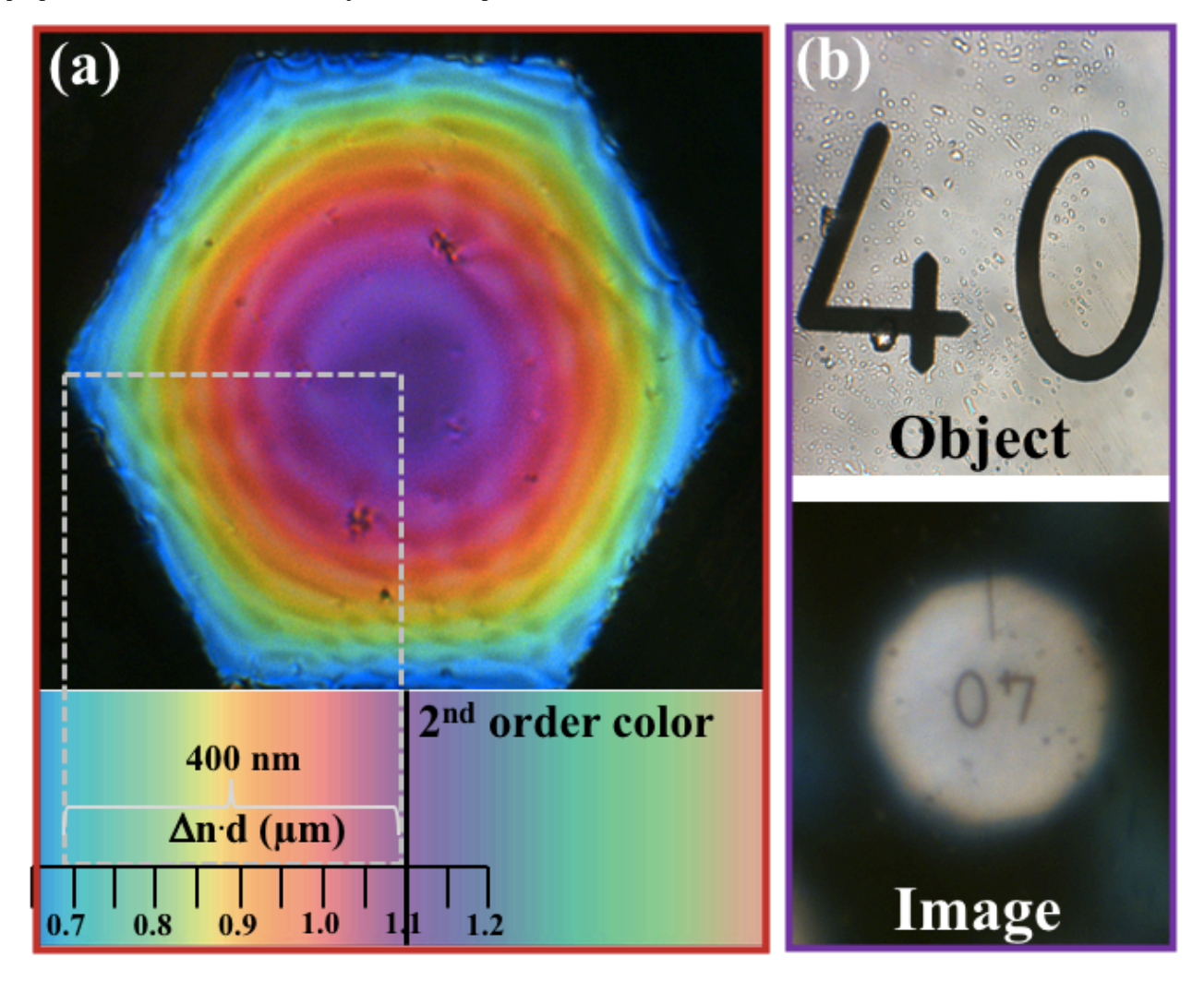


Figure 3: POM image of 5CB doped with 0.1% chiral nanoparticle suspended in a hexagonal grip immersed in water, and the image of an object "40" created by the suspended lens. (a) The POM image with interference color chart with the scale of the optical path difference. (b) Microscopic pictures of the object "40" and its image created by the LC lens.

To summarize, we presented the first spontaneously forming lenses of chiral nanoparticle-doped nematic liquid crystal materials. We found that the helical twisting power of the nanoparticles that is the key factor to form the lens, is an order of magnitude greater than of strongest molecular chiral dopants. From the observations we presented, we were able to estimate the shape and the geometric focal length and also demonstrated the performance of the lens as an optical device. The measurement of focal length at known NP concentration offers new method to measure the helical twisting power of chiral nanoparticles. Additionally, chiral nanoparticles offer the possibility of making microlenses that can be tuned by light adsorbed by the nanoparticles or, for magnetic NPs, by magnetic fields.

ACKNOWLEDGEMENT: This work was supported by NSF DMR-1904091 and 1709985.

REFERENCES

- [1] Li, F., Chen, S., Luo, H. and Gao, Y., "Curved micro lens array for bionic compound eye," Optik (Stuttg). **124**(12), 1346–1349 (2013).
- [2] Commander, L. G., Eastell, C. J., Isherwood, R. and Holmes, B. W., "Optically Variable Devices" (2011).
- [3] Karp, J. H., Tremblay, E. J. and Ford, J. E., "Planar micro-optic solar concentrator," Quantum 18(2), 137–144 (2010).
- [4] Popovic, Z. D., Sprague, R. A. and Connell, G. A., "Technique for monolithic fabrication of microlens arrays.," Appl. Opt. 27(7), 1281–1284 (1988).
- [5] Yabu, H. and Shimomura, M., "Simple fabrication of micro lens arrays," Langmuir 21(5), 1709–1711 (2005).
- [6] Graham-Rowe, D., "Liquid lenses make a splash," Nat. Photonics(9), 2–4 (2006).
- [7] Dong, L., Agarwal, A. K., Beebe, D. J. and Jiang, H., "Adaptive liquid microlenses activated by stimuli-responsive hydrogels.," Nature **442**(7102), 551–554 (2006).
- [8] Xiao, W. and Hardt, S., "An adaptive liquid microlens driven by a ferrofluidic transducer," J. Micromechanics Microengineering **20**(5), 055032 (2010).
- [9] Krupenkin, T., Yang, S. and Mach, P., "Tunable liquid microlens," Appl. Phys. Lett. 82(3), 316–318 (2003).
- [10] Chronis, N., Liu, G., Jeong, K.-H. and Lee, L., "Tunable liquid-filled microlens array integrated with microfluidic network.," Opt. Express 11(19), 2370–2378 (2003).
- [11] Sato, S., "Liquid-crystal lens-cells with variable focal length," Jpn. J. Appl. Phys. 18(9), 1679–1684 (1979).
- [12] Patel, J. S. and Rastani, K., "Electrically controlled polarization-independent liquid crystal Fresnel lens arrays," Opt. Lett. **16**(7), 532–534 (1991).
- [13] Lee, J.-H., Beak, J.-H., Kim, Y., Lee, Y.-J., Kim, J.-H. and Yu, C.-J., "Switchable reflective lens based on cholesteric liquid crystal," Opt. Express 22(8), 9081 (2014).
- [14] Pishnyak, O., Sato, S. and Lavrentovich, O. D., "Electrically tunable lens based on a dual-frequency nematic liquid crystal," Appl. Opt. **45**(19), 4576–4582 (2006).
- [15] Xu, S., Li, Y., Liu, Y., Sun, J., Ren, H. and Wu, S. T., "Fast-response liquid crystal microlens," Micromachines 5(2), 300–324 (2014).
- [16] Lin, Y.-H., Chen, H.-S. and Chen, M.-S., "Electrically Tunable Liquid Crystal Lenses and Applications," Mol. Cryst. Liq. Cryst. **596**(1), 12–21 (2014).
- [17] Kim, Y. H., Jeong, H. S., Kim, J. H., Yoon, E. K., Yoon, D. K. and Jung, H.-T., "Fabrication of two-dimensional dimple and conical microlens arrays from a highly periodic toroidal-shaped liquid crystal defect array," J. Mater. Chem. **20**(31), 6557 (2010).
- [18] Popov, P., Honaker, L. W., Mirheydari, M., Mann, E. K. and Jákli, A., "Chiral nematic liquid crystal microlenses," Sci. Rep. 7(Lc), 1–21 (2017).
- [19] Gao, K., Cheng, H.-H., Bhowmik, A., McGinty, C. and Bos, P., "Nonmechanical zoom lens based on the Pancharatnam phase effect," Appl. Opt. 55(5), 1145 (2016).
- [20] Brown, G. H. and Wolken, J. J., [Liquid crystals and Biological structures], Academic Press, New York (1979).
- [21] Bouligand, Y., Soyer, M. O. and Puiseux-Dao, S., "La structure fibrillaire et l'orientation des chromosomes chez les Dinoflagell??s," Chromosoma **24**(3), 251–287 (1968).
- [22] Bouligand, Y., "Theory of microtomy artefacts in arthropod cuticle," Tissue Cell **18**(4), 621–643 (1986).
- [23] Li, Y., Liu, Y. and Luo, D., "A photo-switchable and photo-tunable microlens based on chiral liquid crystals," J. Mater. Chem. C 7(48), 15166–15170 (2019).
- [24] Mori, T., Sharma, A. and Hegmann, T., "Significant enhancement of the chiral correlation length in nematic liquid crystals by gold nanoparticle surfaces featuring axially chiral binaphthyl ligands," ACS Nano 10(1), 1552–1564 (2016).
- [25] Nemati, A., Shadpour, S., Querciagrossa, L., Mori, T., Zannoni, C. and Hegmann, T., "Highly Sensitive, Tunable Chirality Amplification through Space Visualized for Gold Nanorods Capped with Axially Chiral Binaphthyl Derivatives," ACS Nano 13(9), 10312–10326 (2019).
- [26] Ostovar Pour, S., Rocks, L., Faulds, K., Graham, D., Parchaňský, V., Bouř, P. and Blanch, E. W., "Through-space transfer of chiral information mediated by a plasmonic nanomaterial," Nat. Chem. 7(7), 591–596 (2015).
- [27] Guerrero-Martínez, A., Alonso-Gómez, J. L., Auguié, B., Cid, M. M. and Liz-Marzán, L. M., "From individual to collective chirality in metal nanoparticles," Nano Today 6(4), 381–400 (2011).

- [28] Guerrero-Martínez, A., Auguié, B., Alonso-Gómez, J. L., Džolič, Z., Gómez-Grańa, S., Žinić, M., Cid, M. M. and Liz-Marzán, L. M., "Intense optical activity from three-dimensional chiral ordering of plasmonic nanoantennas," Angew. Chemie Int. Ed. **50**(24), 5499–5503 (2011).
- [29] Nemati, A., Shadpour, S., Querciagrossa, L., Li, L., Mori, T., Gao, M., Zannoni, C. and Hegmann, T., "Chirality amplification by desymmetrization of chiral ligand-capped nanoparticles to nanorods quantified in soft condensed matter," Nat. Commun. 9(1), 1–13 (2018).